PAPER • OPEN ACCESS

Intrinsic winding of braided vector fields in tubular subdomains

To cite this article: Christopher B Prior and Anthony R Yeates 2021 *J. Phys. A: Math. Theor.* **54** 465701

View the article online for updates and enhancements.

You may also like

IOP ebooks™

Bringing together innovative digital publishing with leading authors from the global scientific community.

Start exploring the collection−download the first chapter of every title for free.

Intrinsic winding of braided vector fields in tubular subdomains

Christopher B Prior[*] and Anthony R Yeates

Department of Mathematical Sciences, Durham University, South Road, Durham, DH1 3LE, United Kingdom

E-mail: christopher.prior@durham.ac.uk

CrossMark

Abstract

Braided vector fields on spatial subdomains which are homeomorphic to the cylinder play a crucial role in applications such as solar and plasma physics, relativistic astrophysics, fluid and vortex dynamics, elasticity, and bio-elasticity. Often the vector field's topology—the entanglement of its field lines—is nontrivial, and can play a significant role in the vector field's evolution. We present a complete topological characterisation of such vector fields (up to isotopy) using a quantity called field line winding. This measures the entanglement of each field line with all other field lines of the vector field, and may be defined for an arbitrary tubular subdomain by prescribing a minimally distorted coordinate system. We propose how to define such coordinates, and prove that the resulting field line winding distribution uniquely classifies the topology of a braided vector field. The field line winding is similar to the field line helicity considered previously for magnetic (solenoidal) fields, but is a more fundamental measure of the field line topology because it does not conflate linking information with field strength.

Keywords: topology, fluid dynamics, tubular domains, helicity

(Some figures may appear in colour only in the online journal)

1. Introduction

The entanglement of vector field integral curves (field lines) in tubular subdomains homeomorphic to the cylinder has long been of wide interest. For example, in stellar interiors, twisted

bundles of magnetic field lines—known as magnetic flux ropes—are potentially important for the generation of large scale magnetic fields (Childress and Gilbert 1995, Moffatt and Proctor 1985, Nordlund *et al* 1992, Bao and Yang 2010). In stellar atmospheres such as the Sun's corona, twisted and braided magnetic fields play a crucial role in dynamic phenomena such as coronal heating, jet formation, and coronal mass ejections (Rust and Kumar 1996, Török and Kliem 2005, Wilmot-Smith 2015, Prior and MacTaggart 2016, Yeates and Hornig 2016). Another area where the dynamic entanglement of magnetic field is crucial is the formation of relativistic jets from black holes and neutron stars (Komissarov 1999, Heinz and Begelman 2000, Contopoulos *et al* 2009, Prior and Gourgouliatos 2019).

In thin body elasticity, structures such as ropes, cables, and biopolymers are treated as thin elastic tubes which can be internally twisted and which often react to this twisting by forming looped and knotted structures (Goriely and Tabor 1998, Thompson *et al* 2002, Grason 2009, Starostin and Van der Heijden 2014, Prior and Neukirch 2016). A particularly well known example is plectoneme formation, whereby an elastic tube submitted to increasing twisting becomes unstable and loops at its centre, forming a self-contacting loop. As the twist is further increased the number of loops increase and the tube becomes supercoiled. DNA is an example of a biopolymer which exhibits this supercoiling and where twisting can be applied by optical tweezer experiments e.g. Forth *et al* (2008). Supercoiling acts as a mechanism for large DNA molecules to compactify in order to fit into their local environment (Mullinger and Johnson 1980). In all of these varied systems, a crucial aspect is their inability to disentangle, at least completely. This often informs their physical behaviour, and means that quantifying entanglement is important for understanding the systems themselves.

Motivation for our work comes from the particular context of magnetised plasmas, where the standard tool for quantifying entanglement is a volume integral called magnetic helicity, H (Woltjer 1958, Berger and Field 1984), analogous to a similar quantity in fluid dynamics (Moreau 1961, Moffatt 1969, Arnold and Khesin 1992). For a 'closed' magnetic field whose field line curves are tangent to the boundary, the value of this integral is invariant under an ideal evolution because field lines cannot reconnect and change their topology. As a result, having non-zero H constrains the amount of magnetic energy that can be released (Arnold and Khesin 1992). In such a magnetically-closed volume, it has long been known that H may be written as an average of the Gauss linking integral between all pairs of magnetic field line curves (Pohl 1968, Moffatt 1969, Cantarella and Parsley 2010). Recently, Prior and Yeates (2014) showed that the H admits an analogous interpretation for so-called 'braided' magnetic fields, where magnetic field lines connect between two planar boundaries rather than being tangent. In this case, H is gauge dependent, but the authors showed that there is a particular gauge, the 'winding gauge', in which H is the equal to the average winding number between all pairs of field line curves. This extends the topological interpretation of helicity beyond the restricted case of tangent fields, which are not directly relevant for applications such as stellar atmospheres.

The main limitation of the winding-gauge helicity is that it is defined only for domains foliated by planes, for which the standard definition of winding number can be used. However, in many contexts it would be useful to consider tubular domains of more general shape. One example would be the concentrated magnetic flux ropes that form during flux emergence into the solar atmosphere. Such flux ropes typically occupy curved and distorted domains that cannot be represented as foliations of parallel planes (Longcope and Malanushenko 2008). Yet to characterise the internal entanglement of such structures it is necessary to isolate them from the surrounding magnetic field. Recent work has suggested that these structures may be more stable if they have a complex, 'braided' internal field-line topology, rather than a uniformly twisted structure (Prior and Yeates 2016). Even in stable loops it was shown that different

internal braiding patterns can lead to significantly different internal heating (Wilmot-Smith *et al* 2011). It is important to note that the definition of winding-gauge helicity given in Prior and Yeates (2014) will fail not only if the tubular domain as a whole has a curved shape, but also if its end 'caps' are not flat. Recently it was shown that accounting for such wrinkling of the Sun's surface can significantly affect the measured input of magnetic helicity into the solar atmosphere (Prior and MacTaggart 2019). Observational studies of such helicity injection are important because they can potentially be used try to predict the ensuing behaviour of the atmospheric magnetic field (Romano *et al* 2011, Dalmasse *et al* 2014, Gopalswamy *et al* 2017), as well as providing insight into the unobservable magnetic structure in the solar interior. Thus there is a need to consider winding numbers on more general domains, so as to quantify the entanglement of vector fields on those domains. This is the main aim of this paper.

To fully quantify the entanglement of a braided vector field, it is not sufficient to consider only a single, global integral like magnetic helicity, H. To give an extreme example, since H is a signed quantity, one can have a topologically non-trivial vector field with zero total H, such as the Borromean rings (Del Sordo *et al* 2010) or the equivalent magnetic braid (Wilmot-Smith 2015). Moreover, in real systems that are not perfectly ideal, it is often the case that there are substantial local changes in entanglement, even when the total H (the average entanglement) is conserved to a good approximation (Taylor 1974, Russell *et al* 2015). A full understanding of the field line topology therefore requires the study of finer-grained invariants. As such, our main quantity of interest in this paper is not the analogue of H (which would be the average winding among all pairs of field lines), but rather the analogue of field line helicity (Berger 1988, Yeates and Hornig 2013, Aly 2018, Yeates and Page 2018, Moraitis *et al* 2019). This we call the field line winding, as it is defined for each field line and measures the average winding of this field line with all others.

Our new measure of field line winding allows not only for more general shapes of domain but also for more general classes of vector field. We still assume that the vector field is 'braided' (defined precisely in section 2), but unlike in Prior and Yeates (2014) we do not require it to be solenoidal (divergence free). As will be discussed in section 6, this amounts to removing the field-strength information from the winding measure. Magnetic helicity, for example, has units of magnetic flux squared, and is effectively a confluence of both topological and strength information. As shown in Prior and Yeates (2014), a given set of field line curves can have different helicity depending on the field strength. In this paper, we focus purely on how to uniquely describe the field line topology, without regard to the strength. This unweighted, purely topological measure applies equally to non-solenoidal fields, whereas the magnetic helicity, for example, is an ideal invariant only thanks to the solenoidal nature of the magnetic field.

The paper is organised as follows. After stating our assumptions on the vector field and domain in section 2, we give the general definition of winding numbers and field line winding in section 3. These definitions rely on establishing a least distorted vector field on the domain, whose field lines have no mutual winding. This is addressed in section 4. In section 5, we prove that the field line topology is completely determined by the distribution of field line winding. This is an extension of an earlier completeness result that applied only to a more restricted class of solenoidal vector fields (Yeates and Hornig 2013, Yeates and Hornig 2014, Prior and Yeates 2018). As well as extending the class of domains and vector fields considered, we prove that the field line winding measure uniquely determines not only the field line mapping (as in the earlier papers) but also whether or not the two vector fields can be linked by an ideal evolution (an end-vanishing isotopy). Thus we also strengthen the earlier result for magnetic fields. The relation of our field line winding invariant to magnetic helicity is discussed in section 6, before concluding in section 8.
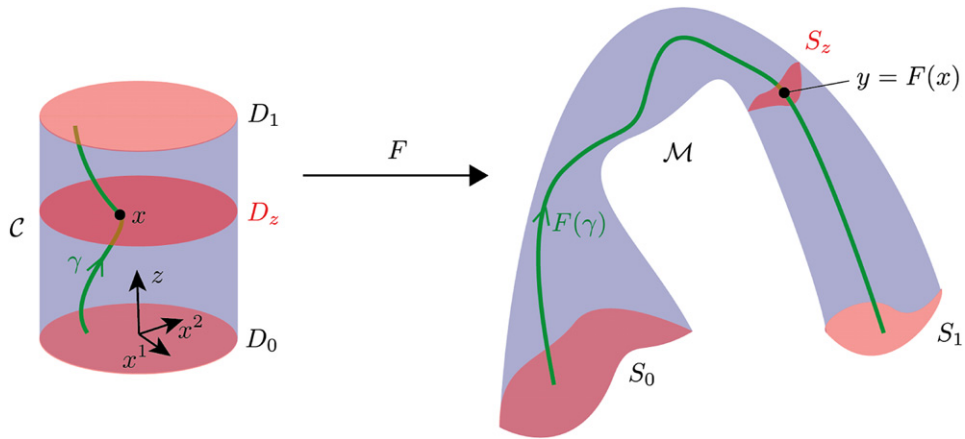
Figure 1. A tubular subdomain $\mathcal{M}$ is an embedding of the unit cylinder in $\mathbb{R}^3$ given by a homeomorphism $F : \mathcal{C} \to \mathbb{R}^3$. The discs D_z of constant z in the cylinder $\mathcal{C}$ map to distorted surfaces S_z that foliate $\mathcal{M}$. Shown in green are a field line $F(\gamma) \in \mathcal{M}$ and its preimage curve $\gamma \in \mathcal{C}$. A crucial part of this study will be to determine a minimally-distorted choice for the map F, within a given subdomain $\mathcal{M}$.

2. Assumptions and notation

In this paper, we consider vector fields $\mathbf{v}$ defined on subdomains $\mathcal{M} \subset \mathbb{R}^3$. Both are restricted, in the following ways. The subdomain $\mathcal{M}$ is 'tubular', meaning that it may be thought of as an embedding of the solid unit cylinder $\mathcal{C}$ in $\mathbb{R}^3$, determined by some homeomorphism $F : \mathcal{C} \to \mathbb{R}^3$, as in figure 1. This homeomorphism F is by no means unique, and an important part of this paper will be to choose a suitable F. Note that the boundary $\partial \mathcal{M} = S_0 \cup S_1 \cup S_s$ is the union of two end caps S_0, S_1 and a side boundary S_s, and this composite boundary is assumed Lipschitz continuous. This means that $\mathcal{M}$ can be foliated by a set of surfaces $S_z, z \in [0, 1]$. We will choose F so that these surfaces are the images of the discs D_z of constant z in $\mathcal{C}$, where we define Cartesian coordinates on $\mathcal{C}$ as (x^1, x^2, z). This notation recognizes the special role of the third coordinate in defining the foliation. In effect, z becomes an axial coordinate for $\mathcal{M}$. Throughout this paper we will denote points in $\mathcal{C}$ by x and points in $\mathcal{M}$ by y.

The vector field $\mathbf{v}$ is 'braided', meaning that it is Lipschitz continuous, non-zero everywhere in $\mathcal{M} \cup \partial \mathcal{M}$, and satisfies the boundary conditions

$$\hat{\mathbf{z}} \cdot \mathbf{v} > 0 \quad \text{on } S_0, \qquad \hat{\mathbf{z}} \cdot \mathbf{v} > 0 \quad \text{on } S_1, \qquad \hat{\mathbf{n}} \cdot \mathbf{v} = 0 \quad \text{on } S_s, \qquad (1)$$

where $\hat{\mathbf{z}}$ is a unit vector normal to S_z pointing in the direction of increasing z and $\hat{\mathbf{n}}$ is the unit normal to S_s. Thus the integral curves/field lines of $\mathbf{v}$ are all rectifiable curves that connect from S_0 to S_1, as shown for the three example field lines in figure 2. The final assumption on $\mathbf{v}$ is that its field lines can be deformed by isotopy to a vector field satisfying $\hat{\mathbf{z}} \cdot \mathbf{v} > 0$ on every S_z. By an isotopy we mean a continuous set of homeomorphisms of the curves (which are automorphisms of the domain $\mathcal{M}$). For such fields, we can define a mapping from S_0 to S_z, or equivalently from D_0 to D_z by following the field lines. These mappings are diffeomorphisms thanks to the Picard–Lindelöf theorem see, e.g. Arnold (2012). In particular, we define a diffeomorphism $f(1)$ from D_0 to D_1 that will be used in section 5.
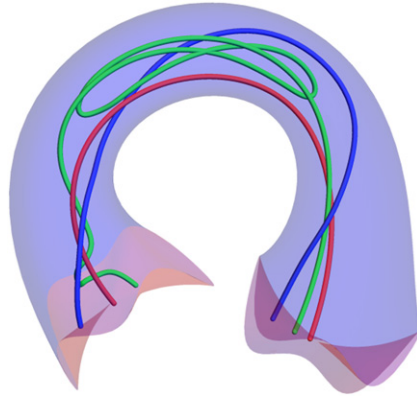
Figure 2. Three curves that could be field lines of a braided vector field as defined in section 2. The green curve would not be monotone in z but is still valid provided that the corresponding **v** can be deformed by isotopy to a field with field lines that are monotone in z.

3. Field line winding

Our goal in this paper is to describe the field-line topology of a braided vector field **v** in $\mathcal{M}$. In other words, properties of the field lines that remain unchanged under a continuous isotopy/deformation of **v**. Since the field lines exit $\mathcal{M}$ through S_0 and S_1, we must qualify this statement: we consider properties that remain invariant under isotopies of **v** *that vanish on S_0 and S_1*. These we call end-vanishing isotopies.

Our topological invariants are based on winding numbers between field lines. In this paper, we take advantage of the embedding of $\mathcal{M}$ and define the winding number between any two curves in $\mathcal{M}$ by calculating the winding number between their two preimage curves in $\mathcal{C}$. An alternative approach would be to work in $\mathcal{M}$ directly by choosing a metric structure. The advantage of our approach is that it allows us to define the angle in a simple and clear manner (i.e. on the cylinder), as well as simplifying the proof in section 5. Figure 3(a) shows field lines of an example vector field on a tubular domain $\mathcal{M}$, and figure 3(b) shows the preimages of these curves in $\mathcal{C}$ for a particular choice of the embedding map F. How best to choose F will be addressed in section 4.

3.1. Pairwise winding number

Given two preimage curves γ, $\widetilde{\gamma}$ in $\mathcal{C}$, the most basic topological invariant is their pairwise winding number. In any plane D_z, we can use the Cartesian components of the two curves γ and $\widetilde{\gamma}$ to define the 'angle' between them,

$$\Theta(\gamma, \widetilde{\gamma}, z) = \arctan\left(\frac{\gamma_2(z) - \widetilde{\gamma}_2(z)}{\gamma_1(z) - \widetilde{\gamma}_1(z)}\right), \tag{2}$$

as shown in figure 4. The net change in this angle as we follow the curves from $z = 0$ to $z = 1$ is the pairwise winding number
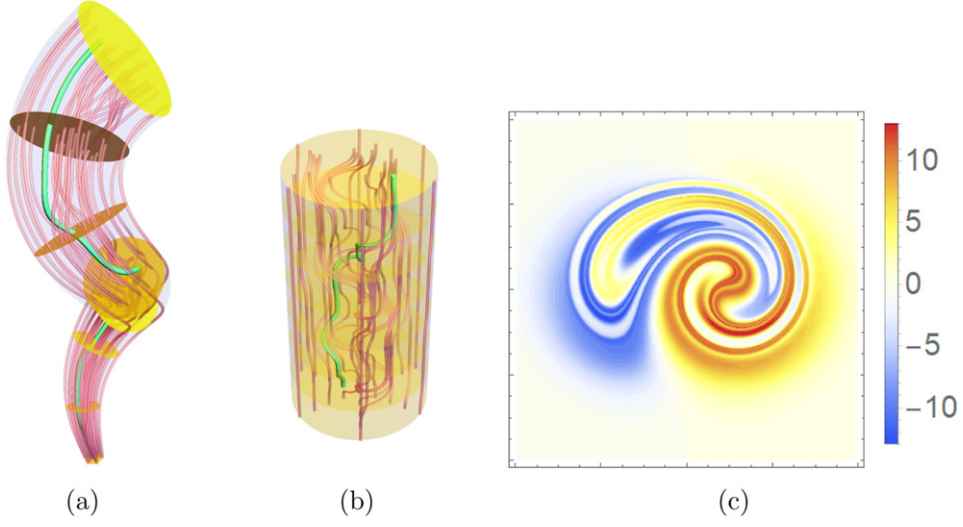
Figure 3. Example illustrating the mapping of field line curves from a tubular domain $\mathcal{M}$ (a) to the cylinder $\mathcal{C}$ (b), along with the resulting distribution of field-line winding $L_{\mathbf{v}}$ in D_0 (c). The green curves in (a) and (b) show a particular field line γ and its preimage. The interpretation of $L_{\mathbf{v}}(\gamma)$ is its average winding number with each of the other curves. Overall, this vector field shows significant entanglement due to the intermixing of positive and negative winding.

$$\mathcal{L}(\gamma, \widetilde{\gamma}) = \frac{1}{2\pi} \int_0^1 \frac{\mathrm{d}}{\mathrm{d}z} \Theta(\gamma, \widetilde{\gamma}, z) \, \mathrm{d}z \tag{3}$$

$$= \frac{1}{2\pi} \int_0^1 \frac{(\gamma_1 - \widetilde{\gamma}_1)\frac{\mathrm{d}}{\mathrm{d}z}(\gamma_2 - \widetilde{\gamma}_2) - (\gamma_2 - \widetilde{\gamma}_2)\frac{\mathrm{d}}{\mathrm{d}z}(\gamma_1 - \widetilde{\gamma}_1)}{(\gamma_1 - \widetilde{\gamma}_1)^2 + (\gamma_2 - \widetilde{\gamma}_2)^2} \, \mathrm{d}z, \tag{4}$$

where primes denote differentiation by z. Alternatively, we may write

$$\mathcal{L}(\gamma, \widetilde{\gamma}) = \frac{1}{2\pi} \left(\Theta(\gamma, \widetilde{\gamma}, 1) - \Theta(\gamma, \widetilde{\gamma}, 0) \right) + N(\gamma, \widetilde{\gamma}), \tag{5}$$

where $N(\gamma, \widetilde{\gamma})$ counts the (signed) number of branch cut crossings as we follow the curves in z. This makes clear that $\mathcal{L}(\gamma, \widetilde{\gamma})$ is invariant under any isotopy of the curves that does not move their end-points. In other words, it is a topological invariant.

Berger and Prior (2006) showed that the definition of $\mathcal{L}(\gamma, \widetilde{\gamma})$ may be generalised to allow for non-monotonic curves like the green curve in figure 2. Such a curve γ is split into $n + 1$ sections $\gamma^{(0)}, \ldots, \gamma^{(n)}$ using the n turning points where $\mathrm{d}\gamma_z/\mathrm{d}z = 0$. For each section, we define the indicator function

$$\sigma^{(i)} = \begin{cases} 1 & \text{if } \mathrm{d}\gamma_z^{(i)}/\mathrm{d}z > 0, \\ -1 & \text{if } \mathrm{d}\gamma_z^{(i)}/\mathrm{d}z < 0, \\ 0 & \text{otherwise.} \end{cases} \tag{6}$$
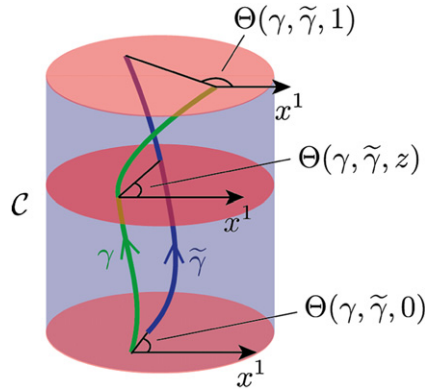
Figure 4. Definition of the angle Θ between two curves $\gamma, \widetilde{\gamma}$ on $\mathcal{C}$.

We split $\widetilde{\gamma}$ and define $\tilde{\sigma}^{(j)}$ in a similar way. Then the pairwise winding number is the sum

$$\mathcal{L}(\gamma, \widetilde{\gamma}) = \sum_{i=0}^{n} \sum_{j=0}^{\tilde{n}} \frac{\sigma^{(i)} \tilde{\sigma}^{(j)}}{2\pi} \int_{z_{ij}^{\min}}^{z_{ij}^{\max}} \frac{\mathrm{d}}{\mathrm{d}z} \Theta(\gamma^{(i)}, \widetilde{\gamma}^{(j)}, z) \, \mathrm{d}z, \tag{7}$$

where $[z_{ij}^{\min}, z_{ij}^{\max}]$ is the mutual range of z values (if any) shared by the curve sections $\gamma^{(i)}$ and $\widetilde{\gamma}^{(j)}$. Once again, $\mathcal{L}(\gamma, \widetilde{\gamma})$ is invariant to any isotopy of the curves that fixes their endpoints. It reduces to (3) if both curves have only a single section stretching from $z = 0$ to $z = 1$. (Although not needed here, Berger and Prior (2006) also showed that when the curves are closed, $\mathcal{L}(\gamma, \widetilde{\gamma})$ is equal to their Gauss linking integral, hence the notation '$\mathcal{L}$'.)

It is important to realize that the value of $\mathcal{L}(\gamma, \widetilde{\gamma})$ depends on the choice of embedding map F. This is illustrated by figure 5. Nevertheless, $\mathcal{L}(\gamma, \widetilde{\gamma})$ is a topological invariant for any (fixed) choice of F, under deformations that vanish on S_0 and S_1.

3.2. Field line winding of a vector field

In principle, we could characterise the field line topology of **v** by the set of all pairwise winding numbers $\mathcal{L}(\gamma, \widetilde{\gamma})$ between all pairs of preimage field lines. However, we will show in section 5 that this would entail significant redundancy. A more succinct description of the field line topology is given by a quantity we call the field line winding. This is defined for each field line γ, and is simply the average winding number of γ with all other field lines in $\mathcal{C}$, i.e.

$$L_{\mathbf{v}}(\gamma) = \int_{D_0} \mathcal{L}(\gamma, \widetilde{\gamma}(x)) \, \mathrm{d}^2 x. \tag{8}$$

Here $\widetilde{\gamma}(x)$ denotes the field line starting from a point $x \in D_0$. Since every field line γ passes through D_0, $L_{\mathbf{v}}$ defines a scalar distribution on D_0. An example of such a distribution is shown in figure 3(c).

By virtue of its definition, $L_{\mathbf{v}}$ is invariant under end vanishing isotopies of **v** that vanish on S_0, S_1. Like $\mathcal{L}(\gamma, \widetilde{\gamma})$, the field line winding $L_{\mathbf{v}}(\gamma)$ is dependent on the choice of mapping from $\mathcal{C}$ to $\mathcal{M}$; we will shortly fix this choice and hence the definition of $\mathcal{L}$.
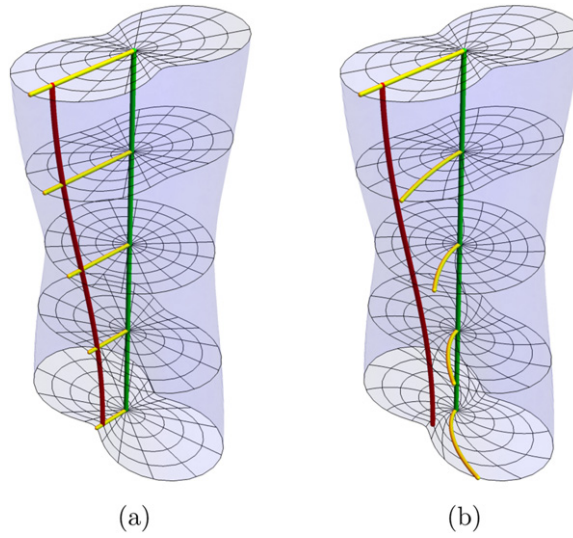
Figure 5. How two different choices of mapping F can lead to different pairwise winding number $\mathcal{L}(\gamma, \widetilde{\gamma})$. Here the red and green curves show $F(\gamma)$ and $F(\widetilde{\gamma})$, while yellow lines indicate the surface that $F(\gamma)$ should belong to in each coordinate system to give constant $\Theta(\gamma, \widetilde{\gamma}, z)$. In (a) $F(\gamma)$ lies in this surface, so $\mathcal{L}(\gamma, \widetilde{\gamma}) = 0$, but in (b) it does not and $\mathcal{L}(\gamma, \widetilde{\gamma}) \neq 0$.

An alternative way to write (8) is to use Cartesian coordinates (x^1, x^2, z) on $\mathcal{C}$, then (4) gives

$$L_{\mathbf{v}}(\gamma) = \frac{1}{2\pi} \int_0^1 \int_{D_z} \frac{(x^1 - \gamma_1)\frac{\mathrm{d}}{\mathrm{d}z}[\widetilde{\gamma}_2(x) - \gamma_2] - (x^2 - \gamma_2)\frac{\mathrm{d}}{\mathrm{d}z}[\widetilde{\gamma}_1(x) - \gamma_1]}{(x^1 - \gamma_1)^2 + (x^2 - \gamma_2)^2} \, \mathrm{d}^2x \, \mathrm{d}z,$$

(9)

where $\widetilde{\gamma}(x)$ is the curve passing through the point $x = (x^1, x^2, z) \in D_z$.

4. Choice of embedding map

For measuring field line winding on a fixed subdomain $\mathcal{M}$, any choice of embedding map F : $\mathcal{C} \to \mathcal{M}$ will generate a topological measure $L_{\mathbf{v}}$ that is invariant under end-vanishing isotopies. However, as we saw in figure 5, the actual value of $L_{\mathbf{v}}$ for each field line depends on the chosen mapping. In order to allow for comparison between vector fields on different $\mathcal{M}$, it is useful to define F uniquely and fix an absolute $L_{\mathbf{v}}$. In this section, we propose to do this by identifying the 'least distorted' vector field on $\mathcal{M}$, that follows the shape of the tube as simply as possible. We then define F so that the field lines of this least distorted field are the images of vertical lines on $\mathcal{C}$. This way, they will all have $L_{\mathbf{v}} \equiv 0$. Vector fields with non-trivial field line topology will then have $L_{\mathbf{v}} \neq 0$, at least for a subset of their field lines.

4.1. The least distorted field

A natural candidate for least-distorted braided vector field on $\mathcal{M}$ is a harmonic vector field $\mathbf{u} = \nabla\phi$ that satisfies

$$\nabla^2\phi = 0 \quad \text{in } \mathcal{M}, \tag{10}$$

$$\hat{\mathbf{z}} \times \nabla\phi = 0 \quad \text{on } S_0, \; S_1, \tag{11}$$

$$\hat{\mathbf{n}} \cdot \nabla\phi = 0 \quad \text{on } S_s. \tag{12}$$

Here we reiterate that $\hat{\mathbf{z}}$ is the unit normal to the cross-sectional surfaces S_z, and $\hat{\mathbf{n}}$ is the unit normal to the side boundary S_s. Conditions (10)–(12) define $\mathbf{u}$ uniquely up to magnitude, disregarding the trivial case of constant ϕ. Condition (11) implies that ϕ is constant on each of the end caps, so that the integral curves are normal to these end caps. The actual values of these two constants control the magnitude and sign of $\mathbf{u}$, but not the shape of its integral curves. That this field can be assumed to exist on $\mathcal{M}$ is a result of theorem 1.1 of Gol'dshtein *et al* (2011), which provides a mixed boundary condition Hodge decomposition on Lipschitz domains. In particular the dimension of the harmonic field space, given by (1.6) in that paper, is 1 for a cylinder; this dimension corresponds to the magnitude of the field $\mathbf{u}$.

To motivate the choice of condition (11), consider any other harmonic field $\nabla\phi' = \nabla(\phi + \psi)$ in $\mathcal{M}$ that satisfies (12) and has the same flux as $\nabla\phi$ through S_0 and S_1, meaning that

$$\int_{S_0} \hat{\mathbf{z}} \cdot \nabla\psi \, \mathrm{d}S = \int_{S_1} \hat{\mathbf{z}} \cdot \nabla\psi \, \mathrm{d}S = 0. \tag{13}$$

It follows from these boundary conditions, and from the constancy of ϕ on S_0 and S_1, that the Dirichlet (stretching) energy of $\nabla\phi'$ is the orthogonal sum

$$\int_{\mathcal{M}} |\nabla\phi'|^2 \, \mathrm{d}V = \int_{\mathcal{M}} |\nabla\phi|^2 \, \mathrm{d}V + \int_{\mathcal{M}} |\nabla\psi|^2 \, \mathrm{d}V. \tag{14}$$

Therefore $\nabla\phi$ is the harmonic field in $\mathcal{M}$ that minimizes this energy for a given axial flux. In this sense, it has the least distorted integral curves. This is related to the notion of harmonic coordinates in Riemannian geometry (DeTurck and Kazdan 1981), which may be thought of as minimizing the Dirichlet energy of a coordinate map from $\mathcal{M}$ to $\mathbb{R}^3$.

Examples of this field $\mathbf{u}$ are shown in figure 6 for various domains, computed using the finite-element code IFEM2 in MATLAB (Chen 2009). Note that the curves of this least distorted field flow through the domain, contouring to its shape and expanding (contracting) when the tube does. They are the natural analogue of straight lines in a Cartesian domain.

4.2. Definition of the embedding map

It is most convenient to specify F^{-1} rather than F itself directly. Our fundamental idea is that field lines of $\mathbf{u}$ should map to vertical lines in $\mathcal{C}$, but this leaves considerable freedom in the choice of F^{-1}, both in the z coordinate (effectively distance along the field lines) and in which field line of $\mathbf{u}$ maps to which vertical line in $\mathcal{C}$.

To set the z coordinate, note that $\mathbf{u} = \nabla\phi$ naturally defines a foliation $\{S_z\}$ of $\mathcal{M}$ by taking each S_ϕ to be the surface $\phi = $ constant. Given the freedom in scaling the magnitude of $\mathbf{u}$, we
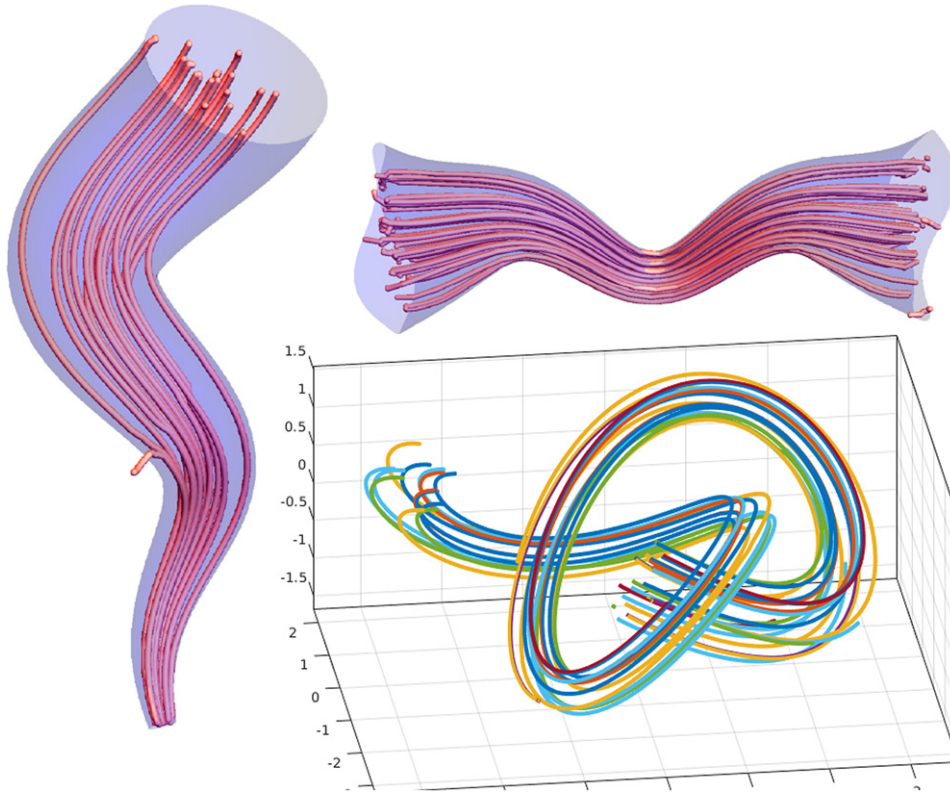
Figure 6. Example domains and computations of their minimally distorted fields **u**.

may always arrange that $\phi = 0$ on S_0 and $\phi = 1$ on S_1. The fact that ϕ gives a valid foliation relies on the fact that **u** is non-zero everywhere on the interior of $\mathcal{M}$ (see appendix A).

Choosing which field line of **u** maps to which vertical line is equivalent to choosing F^{-1} on one of the end caps, say S_0. Equivalently, we must choose functions $(x^1(y), x^2(y))$ for $y \in S_0$. To avoid measuring any spurious pairwise winding (cf figure 5), we require each of the functions x^1 and x^2 to be harmonic in the two-dimensional surface S_0, that is

$$\nabla^2_{S_0} x^1|_{S_0} = \nabla^2_{S_0} x^2|_{S_0} = 0. \tag{15}$$

where $\nabla^2_{S_0}$ indicates the Laplacian operator in the surface S_0. To specify a unique solution we also need to impose boundary conditions on ∂S_0. In order to ensure that F^{-1} (and hence F) is one-to-one, these boundary conditions must take the form $x^1 = \cos(\theta(s)), x^2 = \sin(\theta(s))$, where $\theta(s)$ is an angle function of arclength s along ∂S_0. An example is shown in figure 7, where we make the simple choice $\theta(s) = 2\pi s/L$ for some arbitrary point $s = 0$, where L is the perimeter length of S_0.
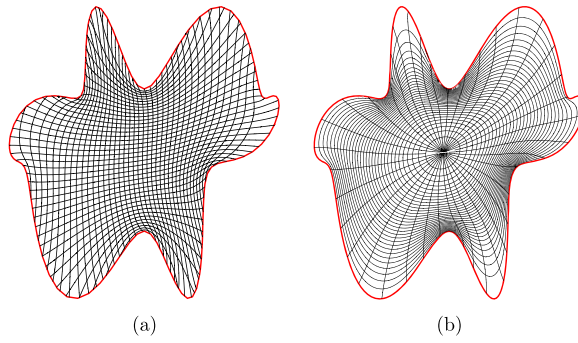
Figure 7. Example illustrating our proposed definition of the mapping F on the lower boundary, S_0. Black lines in (a) show the images under F of x^1 and x^2 contours, whereas those in (b) show the images of polar coordinate (r, θ) contours under the same F.

5. Topological classification

In this section, we will show that the field-line winding $L_\mathbf{v}$ distribution for a braided vector field $\mathbf{v}$ completely determines the topology of its field lines, in the following sense.

Theorem 1. *Let* $\mathbf{v}$, $\mathbf{v}'$ *be two braided vector fields on the same domain* $\mathcal{M}$ *whose field lines on* S_s *are linked by an end-vanishing isotopy. Then the field lines of* $\mathbf{v}$ *and those of* $\mathbf{v}'$ *within* $\mathcal{M}$ *can be linked by an end-vanishing isotopy if and only if* $L_\mathbf{v} = L_{\mathbf{v}'}$ *on all of* D_0.

Notice that this is purely a result about the field line curves: the magnitudes of $\mathbf{v}$ and $\mathbf{v}'$ do not matter, because $L_\mathbf{v}$ and $L_{\mathbf{v}'}$ depend only on the geometry of the curves. The boundary requirement on S_s relates to a fundamental fact regarding the classification group of parametrized diffeomorphisms of the unit disc (Aref 1984, Birman 2016). Essentially, if the corresponding field line mappings $f(1)$, $f'(1)$ differ on the side boundary, then this difference could be compensated by an opposite rotation on the interior, leading to both fields having the same $L_\mathbf{v}$.

Proof of theorem 1. One direction is immediate: we know that $L_\mathbf{v}$ is invariant under any isotopy of $\mathbf{v}$ that vanishes on S_0 and S_1. The other direction is a deeper result. Our strategy will be to first show that equality of $L_\mathbf{v}$ and $L_{\mathbf{v}'}$ implies equality of the corresponding field line mappings $f(1)$, $f(1)'$ from D_0 to D_1. Then, we will show that this implies the existence of an end vanishing isotopy between the field lines of $\mathbf{v}$ and those of $\mathbf{v}'$.

To show equality of the field line mappings $f(1)$ and $f'(1)$, consider the gradient of $L_\mathbf{v}(\gamma)$ with respect to the field line startpoint $(r, \theta) \in D_0$. This is most succinctly expressed in the language of differential forms as $\mathrm{d}_\perp L_\mathbf{v}$, and we claim that

$$\mathrm{d}_\perp L_\mathbf{v} = f^* \alpha - \alpha, \quad \text{where } \alpha(r, \theta, z) = \frac{r^2}{2} \, \mathrm{d}\theta. \tag{16}$$

To see this, note that we can write $L_\mathbf{v}$ in terms of the field line mapping f as

$$L_\mathbf{v}(\gamma) = \int_{D_0} \left[\frac{1}{2\pi} \left(f^* \Theta - \Theta \right) + N(\gamma, \widetilde{\gamma}(x)) \right] \widetilde{r} \, \mathrm{d}^2 x, \tag{17}$$

where $\Theta(\gamma, \widetilde{\gamma}(x), z)$ is the angle made in the surface D_z by the curve γ and another curve $\widetilde{\gamma}$ rooted at a point $x \in D_0$. Treating this as a function of the γ-startpoint $(r, \theta) \in D_0$, we

differentiate to find

$$\mathrm{d}_\perp L_\mathbf{v} = \frac{1}{2\pi} \int_{D_0} \left(f^* \mathrm{d}_\perp \Theta - \mathrm{d}_\perp \Theta \right) \mathrm{d}^2 x. \tag{18}$$

One may show by explicit calculation (see appendix B) that

$$\frac{1}{2\pi} \int_{D_0} \mathrm{d}_\perp \Theta \, \mathrm{d}^2 x = \alpha, \tag{19}$$

from which (16) follows.

Now consider the composite map $g : D_0 \to D_0$, defined by $g = f(1)^{-1} \circ f'(1)$. Under our assumption $L_\mathbf{v} = L_{\mathbf{v}'}$, it follows from equation (16) that $g^* \alpha = \alpha$ (Yeates and Hornig 2013). Equivalently, in components,

$$\frac{g_r^2}{2} \frac{\partial g_\theta}{\partial r} = 0, \qquad \frac{g_r^2}{2} \frac{\partial g_\theta}{\partial \theta} = \frac{r^2}{2}. \tag{20}$$

The first equation shows that $g_\theta(r, \theta) = G(\theta)$, but the fact that $f(1) = f'(1)$ on the side boundary (by our assumption on S_s) means that $g_\theta(r, \theta) = \theta$. The second equation then shows that $g_r(r, \theta) = r$, so g is the identity and hence $f(1) = f'(1)$.

This leaves us to show that there exists an isotopy between any two braided vector fields with the same field line mapping $f(1)$. For this we utilise some established results. The field lines $f(z)$ are parametrised curves in the group of diffeomorphisms of the unit disc, Diffeo(D^2). Since $f(0) = f'(0) = \mathrm{id}$ and $f(1) = f'(1)$, the composite map

$$f_c(z) = \begin{cases} f(z) & z \in [0, 1) \\ f'(2 - z) & z \in [1, 2]. \end{cases} \tag{21}$$

forms a closed curve in this group which is anchored at the identity. If this curve can be shrunk to the identity within the group by a homotopy then the field lines can be linked by an isotopy. Thus we are interested in the homotopy group $\pi_1(\mathrm{Diffeo}(D^2))$ of curves in Diffeo(D^2) (anchored at the identity). A number of established facts related to this group allow us to answer the question. Firstly, there is a restriction map

$$\mathrm{Diffeo}(D^2) \to \mathrm{Diffeo}(S^1), \tag{22}$$

obtained by restricting each diffeomorphism in D^2 to the boundary $\partial D^2 = S^1$. This is a fibration with fibre $\mathrm{Diffeo}_{\partial D^2}(D^2)$, namely diffeomorphisms of the disc that fix the boundary. This implies that the map $\pi_1 \left(\mathrm{Diffeo}((D^2)) \to \pi_1(\mathrm{Diffeo}(S^1)) \right)$ is an isomorphism—see Mann (2013) in conjunction with theorem 4.41 in Hatcher (2002). Finally there is a homotopy equivalence between $\mathrm{Diffeo}(S^1)$ and the group O^2 of rotations (see Smale (1959)). Putting this information together implies that the set of closed curves in the space Diffeo(D^2), from which our map f_c is drawn, can be categorised up to homotopy by their behaviour when restricted to the boundary of the cylinder. Then the fact that the homotopy group has the structure of O^2 implies that closed curves in Diffeo(D^2) are homotopic to the identity if and only if they describe no net integer rotation on the boundary. The boundary assumption in the theorem ensures this for f_c.

$\square$

6. Relation to helicity

Since each pairwise winding number $\mathcal{L}(\gamma, \widetilde{\gamma})$ is itself invariant under end-vanishing isotopies of $\mathbf{v}$, it is clear that any functional

$$W_{\mathbf{v}}(\gamma) = \int_{D_0} w(x)\mathcal{L}(\gamma, \widetilde{\gamma}(x))\mathrm{d}^2x \tag{23}$$

will be similarly invariant. The field line winding $L_{\mathbf{v}}(\gamma)$, with $w \equiv 1$ is the simplest such invariant, and is already sufficient to completely determine the field line topology of $\mathbf{v}$. Nevertheless, there may be situations in which other weightings are of physical interest.

The most notable example is field line helicity, which is defined for the subset of divergence-free braided vector fields. Typical examples are magnetic fields (in magnetohydrodynamics) or vorticity fields. In this section, we shall denote such fields as $\mathbf{b}$ rather than $\mathbf{v}$. The field line helicity is the particular $W_{\mathbf{v}}$ invariant given by

$$A_{\mathbf{b}}(\gamma) = \int_{D_0} J_0(x)b_z(x)\,\mathcal{L}(\gamma, \widetilde{\gamma}(y))\,\mathrm{d}^2x, \tag{24}$$

where J_0 is the Jacobian of the map $F^{-1} : S_0 \to D_0$, and b_z is the normal component of $\mathbf{b}$ on S_0. When $\mathcal{M} = \mathcal{C}$, we have $J_0 \equiv 1$ so

$$A_{\mathbf{b}}(\gamma) = \int_{D_0} b_z(x)\,\mathcal{L}(\gamma, \widetilde{\gamma}(x))\,\mathrm{d}^2x. \tag{25}$$

For this case, Prior and Yeates (2014) showed that (25) is equivalent to the original definition of field line helicity, $A_{\mathbf{b}}(\gamma) = \int_{\gamma} \mathbf{a} \cdot \mathrm{d}\mathbf{l}$ (where $\mathbf{b} = \nabla \times \mathbf{a}$) provided that the vector potential $\mathbf{a}$ is in the so-called winding gauge

$$\mathbf{a}(x^1, x^2, z) = \frac{1}{2\pi} \int_{D_z} \frac{\mathbf{b}(\tilde{x}^1, \tilde{x}^2, z) \times (x^1 - \tilde{x}^1, x^2 - \tilde{x}^2, 0)}{(x^1 - \tilde{x}^1)^2 + (x^2 - \tilde{x}^2)^2}\,\mathrm{d}^2\tilde{x}. \tag{26}$$

Indeed, they used the geometrical interpretation in terms of winding numbers to motivate this particular choice of gauge.

For more general $\mathcal{M}$, we can similarly relate (24) to a particular choice of vector potential. It is convenient to think of $\mathbf{b}$ as a differential two-form $\beta = \mathrm{i}_{\mathbf{b}}\mathrm{vol}^3$ on $\mathcal{M}$, where i is the interior product and vol^3 the volume form (Frankel 2011). Then pushing forward the integral from D_0 to S_0, and using equation (3.13) of Frankel (2011), we have

$$A_{\mathbf{b}}(\gamma) = \int_{S_0} \beta_z(\tilde{y})\mathcal{L}(\gamma, \widetilde{\gamma}(\tilde{y}))\mathrm{d}\tilde{y}^1 \wedge \mathrm{d}\tilde{y}^2 \tag{27}$$

$$= \int_0^1 \int_{S_0} \beta_z(\tilde{y})\frac{\mathrm{d}}{\mathrm{d}z}\Theta(\gamma, \widetilde{\gamma}(\tilde{y}), z)\mathrm{d}\tilde{y}^1 \wedge \mathrm{d}\tilde{y}^2 \mathrm{d}z \tag{28}$$

Now, the divergence free property of $\mathbf{b}$ means that the form $\beta_z\mathrm{d}y^1 \wedge \mathrm{d}y^2$ is conserved along field lines, so we can write

$$A_{\mathbf{b}}(\gamma) = \int_0^1 \int_{S_z} \beta_z(\tilde{y})\frac{\mathrm{d}}{\mathrm{d}z}\Theta(\gamma, \widetilde{\gamma}(\tilde{y}), z)\,\mathrm{d}\tilde{y}^1 \wedge \mathrm{d}\tilde{y}^2\,\mathrm{d}z. \tag{29}$$

Using (4) and the fact that $\mathrm{d}\gamma_i/\mathrm{d}z = \beta_i/\beta_z$, we find that

$$A_{\mathbf{b}}(\gamma) = \int_\gamma \alpha, \tag{30}$$

where the one-form $\alpha = \alpha_1 \mathrm{d}y^1 + \alpha_2 \mathrm{d}y^2 + \alpha_z \mathrm{d}z$ has components

$$\alpha_1(y) = -\frac{\beta_z(\tilde{y})(y^2 - \tilde{y}^2)}{(y^1 - \tilde{y}^1)^2 + (y^2 - \tilde{y}^2)^2} \, \mathrm{d}\tilde{y}^1 \wedge \mathrm{d}\tilde{y}^2, \tag{31}$$

$$\alpha_2(y) = \frac{\beta_z(\tilde{y})(y^1 - \tilde{y}^1)}{(y^1 - \tilde{y}^1)^2 + (y^2 - \tilde{y}^2)^2} \, \mathrm{d}\tilde{y}^1 \wedge \mathrm{d}\tilde{y}^2, \tag{32}$$

$$\alpha_z(y) = \frac{\beta_1(\tilde{y})(y^2 - \tilde{y}^2) - \beta_2(y^1 - \tilde{y}^1)}{(y^1 - \tilde{y}^1)^2 + (y^2 - \tilde{y}^2)^2} \, \mathrm{d}\tilde{y}^1 \wedge \mathrm{d}\tilde{y}^2. \tag{33}$$

This one-form corresponds to a vector potential $\mathbf{a}$ on $\mathcal{M}$ which is the generalisation of the winding-gauge vector potential (26).

Notice that $A_{\mathbf{b}}$ contains no additional topological information compared to $L_{\mathbf{b}}$; the difference is that it weights each field line differently according to b_z. This weighting has physical meaning because $\beta_z \mathrm{d}y^1 \wedge \mathrm{d}y^2$ is preserved along field lines—thus the weighting is a property of the field line as a whole, not just an arbitrary function of the endpoints on S_0. An interesting consequence of the additional weighting is that, although $A_{\mathbf{b}}$ is invariant under end-vanishing isotopies of $\mathbf{b}$ like $L_{\mathbf{b}}$, it may behave differently from $L_{\mathbf{b}}$ if the domain $\mathcal{M}$ changes shape. This remains to be investigated further.

7. Calculating the quantity

The evaluation of $L_{\mathbf{v}}(\gamma)$ assumes we have a tubular field $\mathbf{v}$ on a domain $\mathcal{M}$ (and that it can be represented in the ambient Cartesian coordinate system). One method to perform this evaluation is to represent the field $\mathbf{v}$ on the preimage cylinder as $\mathbf{w} = \mathcal{M}^{-1}\mathbf{v} \in \mathcal{C}$. One can then calculate $L_{\mathbf{v}}(\gamma)$ on the domain $\mathcal{C}$ via a calculation on the field $\mathbf{w}$ which will yield $L_{\mathbf{v}}(\gamma)$. By doing this one can use a single code to perform the winding calculation on a cylindrical mesh. To perform this pull-back we construct a set of local vector fields $\left(\frac{\partial}{\partial x_1}, \frac{\partial}{\partial x_2}, \mathbf{u}\right)$ for the coordinate system $(x_1(z), x_2(z), z)$. (i.e. represent these vector fields in the ambient Cartesian coordinate system). Then the field $\mathbf{v}$ can be written as

$$\mathbf{v} = v_1 \frac{\partial}{\partial x_1} + v_2 \frac{\partial}{\partial x_2} + v_z \mathbf{u}, \tag{34}$$

where the functions (v_1, v_2, v_z) are obtained by solving a matrix equation given the known Cartesian forms of the set $\left(\mathbf{v}, \frac{\partial}{\partial x_1}, \frac{\partial}{\partial x_2}, \mathbf{u}\right)$. Note that the set $\left(\frac{\partial}{\partial x_1}, \frac{\partial}{\partial x_2}, \mathbf{u}\right)$ is not necessarily orthogonal, although by definition $\frac{\partial}{\partial x_1}$ and $\frac{\partial}{\partial x_2}$ are normal to $\mathbf{u}$. The functions (v_1, v_2, v_z) represent components of the field $\mathbf{w}$ in a Cartesian coordinate system for $\mathcal{C}$ (which can then be converted to cylindrical coordinates if needs be). Once the components (v_1, v_2, v_z) of $\mathbf{w}$ have been obtained one simply needs to calculate the winding for a vector field in the cylindrical domain $\mathcal{C}$. Descriptions of how this can be done can be found in (Prior and Yeates 2018, Gekelman *et al* 2020) but briefly one can use formula (4) noting that $v_1/v_z = \mathrm{d}\gamma_1/\mathrm{d}z$ and $v_2/v_z = \mathrm{d}\gamma_2/\mathrm{d}z$. Thus, computationally, most of the novelty here is associated with calculating the fields $\frac{\partial}{\partial x_i}, i \in 1, 2$. This can be done via the following steps all of which can be conducted in the ambient Cartesian coordinate system in which $\mathcal{M}$ is embedded:

(a) Calculate the least distorted field **u** by solving the problem defined by equations (10)–(12), a finite element method, as used for the examples in figure 6, will allow for arbitrary $\mathcal{M}$. One can, for example, use the method detailed in Persson and Strang (2004) to generate a mesh for $\mathcal{M}$.

(b) Construct the transverse coordinate system of the bounding surface S_0 as shown in figure 7. This involves solving Laplace's equation (15) on the surface S_0, subject to the boundary conditions described in section 4.2. In general this requires solving Laplace's equation on a non-Euclidean surface, as such an implicit method like the closest point method (Macdonald and Ruuth 2010) might be beneficial.

(c) The vector field $\frac{\partial}{\partial x_1}$, for example, can be approximated by choosing a pair of coordinates $(x_1(0), x_2(0))$ and $(x_1(0) + dx, x_2(0))$ defining points in S_0. The dx here means a small step along the coordinate system $(x_1(0), x_2(0))$ spanning S_0 (i.e. along a curve of constant $x_2(0)$). We can then trace the integral curves $\mathbf{r}[x_1(0), x_2(0)](z)$ of **u** emanating from these points by solving the o.d.e.

$$\frac{d\mathbf{r}}{dz}[x_1(0), x_2(0)](z) = \frac{\mathbf{u}}{\mathbf{u} \cdot \mathbf{u}}, \qquad (35)$$

with the functional argument indicating that $\mathbf{r}[x_1(0), x_2(0)](0)$ will be the Cartesian coordinates of the point defined by $(x_1(0), x_2(0), 0)$ in the ambient coordinate system. Dividing by $\mathbf{u} \cdot \mathbf{u}$ ensures that the curves will advance to the same surfaces of constant z coordinate value in the folidation defined by the field **u**, as $\nabla z = \mathbf{u}$ (see e.g. Frankel (2011) chapter 2.1(e)). Then, for any $z > 0$, we can obtain the following finite difference estimate for $\frac{\partial}{\partial x_1}$:

$$\frac{\mathbf{r}[x_1(0), x_2(0)](z) - \mathbf{r}[x_1(0) + dx, x_2(0)](z)}{dx}. \qquad (36)$$

Thus one can construct the vector fields $\frac{\partial}{\partial x_1}$ and $\frac{\partial}{\partial x_2}$ on surfaces of constant z in the minimal coordinate system, as required to obtain the functions (v_1, v_2, v_z).

8. Conclusions and comparison to other work

The primary development in this work (theorem 1) is the proof of a topological classification theorem for braided vector fields on tubular subdomains, which are homeomorphic to the cylinder as defined in section 4. Specifically, the field lines of a given braided field may be continuously deformed into those of another other field—without moving their endpoints—if and only if the two fields have the same distribution of field line winding, $L_\mathbf{v}$. There is a small caveat: this invariant cannot distinguish overall full (integer) rotations. These could be detected solely from the field line mappings on the side boundary, and are unlikely to be problematic in practical applications. Our result strengthens an earlier theorem of Yeates and Hornig (2014) and extends it to a broader class of vector fields; specifically to include those which have divergence. The measure $L_\mathbf{v}$ has recently been applied to study reconnection in a laboratory plasma experiments (Prior and Yeates 2018, Gekelman *et al* 2020); here we have formalised the underpinning result and extended it to tubular sub-domains that cannot be foliated by parallel planes, including tubular domains foliated by non-Euclidean surfaces.

The unique definition of $L_\mathbf{v}$ relies on the identification of a least distorted vector field **u**, defined in section 4.1, whose integral curves are mapped to straight lines on the cylinder (on

which the field line winding is defined). Our choice of **u** and its mapping to the cylinder have three critical properties:

(a) The vector field **u** minimises the Dirichlet (distortion) energy among all braided vector fields on a given tubular domain $\mathcal{M}$ with a specified flux, i.e. it minimises

$$E = \int_{\mathcal{M}} \mathbf{v} \cdot \mathbf{v} \, \mathrm{d}V, \quad \text{for specified} \int_{S_0} \hat{\mathbf{z}} \cdot \mathbf{v} \, \mathrm{d}S. \tag{37}$$

The latter constraint relates to the fact the energy varies with flux for a fixed topology, whereas we are interested purely in finding the vector field of least entangled topology.

(b) In this mapping, all field lines of **u** have zero pairwise winding number, so the winding measure $L_{\mathbf{v}}$ is everywhere zero for **u** itself.

(c) To determine which field line of **u** maps to which vertical line on $\mathcal{C}$, we use harmonic coordinates so as to avoid the erroneous measurement of entanglement such as in figure 5.

The combination of these three properties means that a non-trivial distribution $L_{\mathbf{v}}$ necessarily indicates non-trivial internal entanglement of the original vector field **v**. This entanglement may be seen as increasing the energy above the minimum level enforced by the distorted global shape of the domain $\mathcal{M}$ itself. The only comparable construction to this of which we are aware is the so-called Mermin–Ho basis, which is defined on a pre-determined Riemannian manifold. Using the notion of parallel transport with respect to a preferred vector field (not specifically assigned in the theory) one can define a local basis on the manifold from which any local deviations of an arbitrary vector from this field are quantified (Mermin and Ho 1976, Kamien 2002). Our work differs in that we define and justify the choice of a preferred vector field. Moreover, this justification is based on a globally defined notion (the winding rate $\mathrm{d}\Theta(\gamma, \widetilde{\gamma}, z)/\mathrm{d}z$), rather than a local notion (parallel transport). The Godbillion–Vey invariant see e.g. (Arnold and Khesin 1992), can be related to the helicity of the integral curves of the foliation of a **closed** domain so is not directly comparable here (see Webb *et al* (2014) for a discussion of its applicability in MHD contexts). Finally we mention that the field line helicity 25 can be formally written as the canonical Hamiltonian (Yeates and Hornig 2014, Prior and Yeates 2018), and thus is formally equivalent to the Calabi invariant of disc diffeomorphisms (Kudryavtseva 2014). Our work here demonstrates that $L_{\mathbf{v}}$ which applied to a larger class of fields and as such is more fundamental.

The invariant $L_{\mathbf{v}}$ used in our classification theorem provides a fundamental description of the field line topology, in the sense that it depends only on the integral curves of the vector field and not on its magnitude or flux. This is in contrast to the widely used (field line) helicity invariants for divergence-free fields (Webb *et al* 2014, Russell *et al* 2015, Cantarella and Parsley 2010, Yeates and Page 2018, Moraitis *et al* 2019), which do depend on the flux. Indeed, we showed in section 6 that the field line helicity—effectively, the helicity of an infinitesimal flux tube surrounding a single field line—takes a similar integral form to $L_{\mathbf{v}}$ but with an additional weighting of flux. As such, it mixes a purely topological quantity (the pairwise winding) with a physical quantity (the flux). This indicated the invariance of helicity under Euler flows (ideal motions) which vanish at the domain boundaries requires not only the invariance of $\mathcal{L}(\gamma, \widetilde{\gamma})$ but also the divergence-free condition, which ensures preservation of flux. Since the flux can change without altering the field line topology, $L_{\mathbf{v}}$ is revealed as a more fundamental quantity than the (field line) helicity. It has recently been shown that this additional decomposition of the magnetic (field line) helicity into topological (winding) and strength components can in provide additional practical information for diagnosing the changing/emerging topology of magnetic fields (Prior and MacTaggart 2019, Prior and MacTaggart 2020,

Gekelman *et al* 2020, MacTaggart and Prior 2021): such as the identification of the underlying topological structure of emerging magnetic fields into the solar corona.

One significant potential application of this categorization theorem is to both magnetic and fluid vortex reconnection. If we have a field $\mathbf{v}(t)$ evolving in time on a given domain $\mathcal{M}$ then we can calculate the distribution of $L_{\mathbf{v}}(\gamma)$ across all field lines (i.e. on C_0), as a function of time. If this distribution changes in time it must mean the field has changed connectivity (assuming no change at its ends). Reconnection of magnetic fields or fluid vortex lines is a typically a local phenomenon, so if the time step separating $\mathbf{v}(t)$ and $\mathbf{v}(t + dt)$ is sufficiently small, the change to the distribution $L_{\mathbf{v}}(\gamma)$ due to reconnection over the time dt will be spatially localised. That is to say if dt is small enough one can identify the regions of (and amount) of changing field connectivity from the changing distribution $L_{\mathbf{v}}$. This exact procedure was used in (Prior and MacTaggart 2019, Gekelman *et al* 2020) to characterise and quantify the reconnective activity in reconnective plasma experiments conducted in cylindrical domains at the UCLA basic plasma facility. The results presented here serve to, (a) provide a theoretical underpinning to the measures used in these studies, and (b) extend the method to a far wider variety of domains and hence potential applications.

One final point of discussion is whether the measure $L_{\mathbf{v}}(\gamma)$ is applicable to closed tubular domains e.g. a torus or knotted tube. One can use the measure $L_{\mathbf{v}}(\gamma)$ on such domains by choosing on cross-sectional surface to represent the starting surface S_0. One issue with this procedure that the distribution would look different depending on the surface chosen. However, for tracking reconnective activity in a time-dependent field evolution it would only matter that this choice is consistent, as it is the change in the distribution that is to be monitored. A second issue is that for example ergodic curves on such domains (excluded in open domains by our assumptions, but not if the domain is closed), mean that the notion that a single point in S_0 corresponds to a single curve becomes invalid. This is not necessarily a problem but one might need to recognise that the ergodic field line can change connectivity with itself at distinct non local points along its length. Finally, for an isotopic evolution of the field (in a closed domain) there would be motion at the bounding caps S_0/S_1 (which are artificially chosen in the closed case). That is to say the distribution $L_{\mathbf{v}}(\gamma)$ would change under isotopy. This motion can be accounted for if the isotopic motion is known. For example in plasma models this isotopic motion is the plasma ion velocity, and it can be measured in experiments, as discussed in Prior and MacTaggart (2019), Gekelman *et al* (2020). In those studies the domain was cylindrical but there was isotopic end motion, and a procedure to extract the change in the $L_{\mathbf{v}}(\gamma)$ due to isotopic boundary motions was constructed. Once this change is removed and other change must be due to reconnective changes in the field. In the closed case this same procedure can be applied at the chosen bounding caps S_0/S_1.

Data availability statement

Appendix A. Validity of the foliation defined by u

In this appendix we show that the least-distorted harmonic field $\mathbf{u}$ defines a valid foliation of the domain $\mathcal{M}$. In particular, we will show that $\mathbf{u} \neq \mathbf{0}$ everywhere on the interior of $\mathcal{M}$, so that there is a unique surface S_z through all interior points and the winding integrals are well defined. It is possible to have points with $\mathbf{u} = \mathbf{0}$ on the boundary ∂M, but these do not prevent the existence of the foliation.
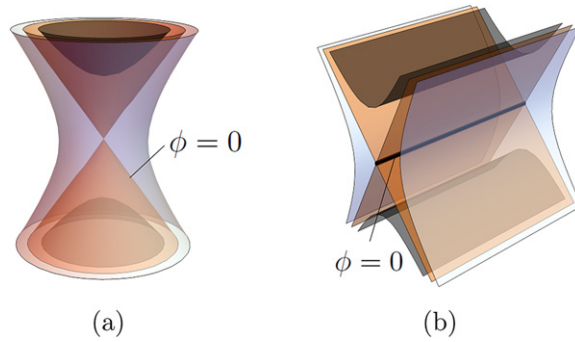
Figure A1. Possible local structures of the constant-ϕ surfaces around null points of harmonic fields $\mathbf{u} = \nabla\phi$. There are two possibilities, depending on whether the null point is isolated (a) or part of a null line (b).

To rule out null points of our harmonic field $\mathbf{u} = \nabla\phi$, the idea is to consider the possible structures of constant-ϕ surfaces that could result from such points, and show that such surfaces cannot exist. If p is a hypothetical point where $\mathbf{u}(p) = \mathbf{0}$, then the local linearisation of $\mathbf{u}$ around p is constrained by the fact that $\mathbf{u}$ is harmonic. Firstly, the tensor $\mathbf{u}$ is symmetric due to $\nabla \times \mathbf{u} = \mathbf{0}$, meaning that it has real eigenvalues λ_1, λ_2, λ_3. Secondly, it is traceless due to $\nabla \cdot \mathbf{u} = 0$, so that $\lambda_1 + \lambda_2 + \lambda_3 = 0$. There are two possible structures around p, shown in figure A1. If all three eigenvalues are non-zero, then in suitable local coordinates we may write

$$\mathbf{u} = \nabla\phi \approx \pm(x, y, -2z), \quad \text{so} \ \ \phi \approx \pm\frac{1}{2}\left(x^2 + y^2 - 2z^2\right). \tag{A.1}$$

Then the surface $\phi = 0$ has the topology of two cones whose tips meet at p (figure A1(a)), separating two-sheet hyperboloids with $\phi > 0$ and one-sheet hyperboloids with $\phi < 0$. Alternatively, if one eigenvalue is 0 then p is part of a null line (figure A1(b)) and, again in suitable local coordinates, we may write

$$\mathbf{u} = \nabla\phi = \pm(x, 0, -z), \quad \text{so} \ \ \phi = \pm\left(x^2 - z^2\right). \tag{A.2}$$

The $\phi = 0$ surface is then a pair of intersecting planes. The null line could either be a closed loop or could intersect the boundary $\partial\mathcal{M}$. It is not possible to have a null surface, nor for all three eigenvalues to vanish at p (unless $\mathbf{u} = \mathbf{0}$ on the whole domain).

To rule out null points and lines, we must consider how the ϕ surfaces extend outside the neighbourhoods of these structures. To do so, we use the fact that ϕ defines a continuous foliation of $\mathcal{M}$ everywhere outside the null set $\mathcal{N} = \{p \in \mathcal{M} | \mathbf{u}(p) = \mathbf{0}\}$. This follows from the Frobenius theorem. So the $\phi = 0$ surfaces from null points or lines extend smoothly away from these locations and can end only on $\mathcal{N}$ or on the boundary $\partial\mathcal{M}$. In fact, they can only intersect (transversely) the side boundary S_s, owing to the boundary conditions of constant ϕ on S_0 and S_1.

Consider first a single null point in the interior, as in figure A2(a). Each of the two $\phi = 0$ surfaces must either be closed or end on S_s (as shown in figure A2(a)). To show that neither is possible, let $\hat{\mathbf{n}}$ be the outward normal from the indicated volume $\mathcal{V}$. Then observe that $\hat{\mathbf{n}} \cdot \mathbf{u}$ is non-zero with the same sign everywhere on these two surfaces where they bound $\mathcal{V}$, because $\phi < 0$ on one side and $\phi > 0$ on the other. Since the two surfaces intersect S_s, and since
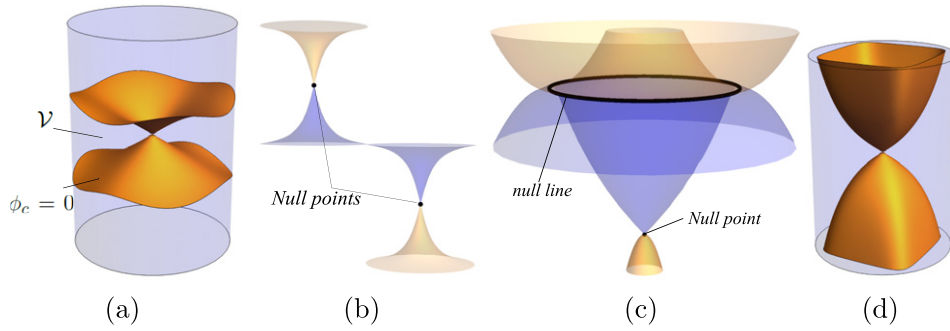
Figure A2. Global extensions of the $\phi = 0$ surfaces from (a) an isolated null point, (b) two isolated null points, and (c) a null point and a null line. In (a), the surfaces intersect the side boundary S_s, enclosing a volume $\mathcal{V}$. In (d) the $\phi = 0$ surface intersects S_0 and S_1 transversely, but this is forbidden by the boundary conditions $\phi = $ constant on S_0 and S_1.

$\hat{\mathbf{n}} \cdot \mathbf{u} = 0$ on S_s, there must be a net flux in/out of $\mathcal{V}$, contradicting $\nabla \cdot \mathbf{u} = 0$. If the surface were closed instead of intersecting S_s, we would similarly obtain a contradiction. So a single null point in the interior cannot exist.

This argument extends to rule out multiple null points or lines in the interior (of which there can only be a countable number). Tracing the $\phi = 0$ surfaces from some null point or line, we can extend these surfaces, possibly incorporating further points in $\mathcal{N}$—as depicted in figures A2(b) or (c)—until the composite surfaces either close on themselves or intersect S_s. Either way we can find a finite volume enclosed with a non-zero flux of $\mathbf{u}$ through its boundary, which contradicts $\nabla \cdot \mathbf{u} = 0$.

Finally we point out that since the boundary is Lipschitz continuous it is possible to embed the conic structure of a null surface $\phi = 0$ in the boundary. As an example this would be necessary on the bounding curves $\partial S_{0/1}$ for an hourglass domain morphology, owing to the boundary conditions on $\mathbf{u}$.

Appendix B. Derivation of equation (19)

To evaluate the left-hand side of (19) at the point $x_0 = (r, \theta)$, consider the components of $d_\perp \Theta$ in polar coordinates (r, θ). Differentiating the expression (2) for $\Theta(x_0, x, z)$ gives

$$\frac{\partial \Theta}{\partial r} = \frac{(x_0^1 - x^1) \sin \theta - (x_0^2 - x^2) \cos \theta}{(x_0^1 - x^1)^2 + (x_0^2 - x^2)^2}, \tag{B.1}$$

$$\frac{\partial \Theta}{\partial \theta} = r \frac{(x_0^1 - x^1) \cos \theta + (x_0^2 - x^2) \sin \theta}{(x_0^1 - x^1)^2 + (x_0^2 - x^2)^2}. \tag{B.2}$$

To evaluate the integrals, change from (x^1, x^2) to polar coordinates centred at x_0,

$$x^1 = \rho \cos \varphi + x_0^1, \qquad x^2 = \rho \sin \varphi + x_0^2. \tag{B.3}$$

In these coordinates,

$$\frac{\partial \Theta}{\partial r} = \frac{\sin(\varphi - \theta)}{\rho}, \qquad \frac{\partial \Theta}{\partial \theta} = -r \frac{\cos(\varphi - \theta)}{\rho}. \tag{B.4}$$

Integrating with respect to (ρ, φ) we must account for the fact that the ρ limit of integration is a function of φ. Substituting expressions (B.3) into the equation $(x^1)^2 + (x^2)^2 = 1$ for the boundary leads to the integration limit

$$\rho(\varphi) = -r \cos(\varphi - \theta) + \sqrt{r^2 \cos^2(\varphi - \theta) - r^2 - 1}. \tag{B.5}$$

Using the phase behaviour of sin and cos, we may then evaluate

$$\frac{1}{2\pi} \int_{D_0} \frac{\partial \Theta}{\partial r} \rho \mathrm{d}\rho \, \mathrm{d}\varphi = \frac{1}{2\pi} \int_0^{2\pi} \sin(\varphi - \theta) \rho(\phi) \, \mathrm{d}\varphi = 0 \tag{B.6}$$

and

$$\frac{1}{2\pi} \int_{D_0} \frac{\partial \Theta}{\partial \theta} \rho \mathrm{d}\rho \mathrm{d}\varphi = \frac{r}{2\pi} \int_0^{2\pi} \cos^2(\varphi - \theta) \, \mathrm{d}\varphi = \frac{r}{2}. \tag{B.7}$$

ORCID iDs

Christopher B Prior ⬤ https://orcid.org/0000-0003-4015-5106

References

Aly J-J 2018 *Fluid Dyn. Res.* **50** 011408
Aref H 1984 *J. Fluid Mech.* **143** 1–21
Arnold V I 2012 *Geometrical Methods in the Theory of Ordinary Differential Equations* vol 250 (Berlin: Springer)
Arnold V I and Khesin B A 1992 *Annu. Rev. Fluid Mech.* **24** 145–66
Bao J and Yang Q 2010 *Nonlinear Dyn.* **61** 773–81
Berger M A and Field G B 1984 *J. Fluid Mech.* **147** 133–48
Berger M A and Prior C 2006 *J. Phys. A: Math. Gen.* **39** 8321
Berger M 1988 *Astron. Astrophys.* **201** 355–61
Birman J S 2016 *Braids, Links, and Mapping Class Groups (AM-82)* vol 82 (Princeton, NJ: Princeton University Press)
Cantarella J and Parsley J 2010 *J. Geom. Phys.* **60** 1127–55
Chen L 2009 *iFEM: an innovative finite element methods package in MATLAB*
Childress S and Gilbert A D 1995 *Stretch, Twist, Fold: The Fast Dynamo* vol 37 (Berlin: Springer)
Contopoulos I, Christodoulou D M, Kazanas D and Gabuzda D C 2009 *Astrophys. J.* **702** L148
Dalmasse K, Pariat E, Démoulin P and Aulanier G 2014 *Sol. Phys.* **289** 107–36
Del Sordo F, Candelaresi S and Brandenburg A 2010 *Phys. Rev.* E **81** 036401
DeTurck D M and Kazdan J L 1981 *Ann. Sci. École Norm. Supér.* **14** 249–60
Forth S, Deufel C, Sheinin M Y, Daniels B, Sethna J P and Wang M D 2008 *Phys. Rev. Lett.* **100** 148301
Frankel T 2011 *The Geometry of Physics: An Introduction* (Cambridge: Cambridge University Press)
Gekelman W, DeHaas T, Prior C and Yeates A 2020 *SN Appl. Sci.* **2** 1–15
Gol'dshtein V, Mitrea I and Mitrea M 2011 *J. Math. Sci.* **172** 347–400
Gopalswamy N, Akiyama S, Yashiro S and Xie H 2017 *Proc. Int. Astron. Union* **13** 258–62
Goriely A and Tabor M 1998 *Phys. Rev. Lett.* **80** 1564
Grason G M 2009 *Phys. Rev.* E **79** 041919
Hatcher A 2002 *Algebraic Topology* (Cambridge: Cambridge University Press)
Heinz S and Begelman M C 2000 *Astrophys. J.* **535** 104
Kamien R D 2002 *Rev. Mod. Phys.* **74** 953
Komissarov S S 1999 *Mon. Not. R. Astron. Soc.* **308** 1069–76
Kudryavtseva E A 2014 *Math. Notes* **95** 877–80

Longcope D W and Malanushenko A 2008 *Astrophys. J.* **674** 1130–43
Macdonald C B and Ruuth S J 2010 *SIAM J. Sci. Comput.* **31** 4330–50
MacTaggart D and Prior C 2021 *Geophys. Astrophys. Fluid Dyn.* **115** 85–124
Mann K 2013 *New York J. Math* **19** 583–96
Mermin N D and Ho T-L 1976 *Phys. Rev. Lett.* **36** 594
Moffatt H K 1969 *J. Fluid Mech.* **35** 117–29
Moffatt H K and Proctor M R E 1985 *J. Fluid Mech.* **154** 493–507
Moraitis K, Pariat E, Valori G and Dalmasse K 2019 *Astron. Astrophys.* **624** A51
Moreau J 1961 *C. R. Acad. Sci. Paris* **252** 2810–2
Mullinger A M and Johnson R T 1980 *J. Cell Sci.* **46** 61–86
Nordlund A, Brandenburg A, Jennings R L, Rieutord M, Ruokolainen J, Stein R F and Tuominen I 1992
    Astrophys. J. **392** 647–52
Persson P-O and Strang G 2004 *SIAM Rev.* **46** 329–45
Pohl W 1968 *Indiana Univ. Math. J.* **17** 975–85
Prior C B and Neukirch S 2016 *J. Phys. A: Math. Theor.* **49** 215201
Prior C and Gourgouliatos K N 2019 *Astron. Astrophys.* **622** A122
Prior C and MacTaggart D 2016 *Geophys. Astrophys. Fluid Dyn.* **110** 432–57
Prior C and MacTaggart D 2019 *J. Plasma Phys.* **85** 775850201
Prior C and MacTaggart D 2020 *Proc. R. Soc.* A **476** 20200483
Prior C and Yeates A R 2014 *Astrophys. J.* **787** 100
Prior C and Yeates A R 2016 *Astron. Astrophys.* **591** A16
Prior C and Yeates A R 2018 *Phys. Rev.* E **98** 013204
Romano P, Pariat E, Sicari M and Zuccarello F 2011 *Astron. Astrophys.* **525** A13
Russell A J B, Yeates A R, Hornig G and Wilmot-Smith A L 2015 *Phys. Plasmas* **22** 032106
Rust D M and Kumar A 1996 *Astrophys. J. Lett.* **464** L199
Smale S 1959 *Proc. Am. Math. Soc.* **10** 621–6
Starostin E L and Van der Heijden G H M 2014 *J. Mech. Phys. Solids* **64** 83–132
Taylor J B 1974 *Phys. Rev. Lett.* **33** 1139–41
Thompson J M T, van der Heijden G H M and Neukirch S 2002 *Proc. R. Soc.* A **458** 959–85
Török T and Kliem B 2005 *Astrophys. J.* **630** L97
Webb G M, Dasgupta B, McKenzie J F, Hu Q and Zank G P 2014 *J. Phys. A: Math. Theor.* **47** 095501
Wilmot-Smith A L 2015 *Phil. Trans. R. Soc.* A **373** 20140265
Wilmot-Smith A L, Pontin D I, Yeates A R and Hornig G 2011 *Astron. Astrophys.* **536** A67
Woltjer L 1958 *Proc. Natl Acad. Sci.* **44** 489–91
Yeates A R and Hornig G 2013 *Phys. Plasmas* **20** 012102
Yeates A R and Hornig G 2014 *J. Phys.: Conf. Ser.* **544** 012002
Yeates A R and Hornig G 2016 *Astron. Astrophys.* **594** A98
Yeates A R and Page M H 2018 *J. Plasma Phys.* **84** 775840602